Human Molecular Genetics, 2003, Vol. 12, No. 16 **2049–2061**
DOI: 10.1093/hmg/ddg210

Claudin 14 knockout mice, a model for autosomal recessive deafness *DFNB29*, are deaf due to cochlear hair cell degeneration

Tamar Ben-Yosef[1], Inna A. Belyantseva[1], Thomas L. Saunders[2], Elizabeth D. Hughes[2], Kohei Kawamoto[3,†], Christina M. Van Itallie[4], Lisa A. Beyer[3], Kärin Halsey[3], Donald J. Gardner[5], Edward R. Wilcox[1], Julia Rasmussen[6], James M. Anderson[6], David F. Dolan[3], Andrew Forge[7], Yehoash Raphael[3], Sally A. Camper[2] and Thomas B. Friedman[1,*]

[1]Laboratory of Molecular Genetics, National Institute on Deafness and Other Communication Disorders, National Institutes of Health, Rockville, MD 20850, USA, [2]Department of Internal Medicine, Division of Molecular Medicine and Genetics, University of Michigan, Ann Arbor, MI 48109-0638, USA, [3]Kresge Hearing Research Institute, University of Michigan Medical School, Ann Arbor, MI 48109-0648, USA, [4]Department of Medicine, UNC at Chapel Hill, Chapel Hill, NC 27599, USA, [5]Veterinary Resources Program, National Institutes of Health, Bethesda, MD, USA, [6]Department of Cell and Molecular Physiology, UNC at Chapel Hill, Chapel Hill, NC 27599, USA and [7]UCL Centre for Auditory Research and Institute of Laryngology and Otology, University College London, London WC1X 8EE, UK

Received May 2, 2003; Revised and Accepted June 16, 2003

Tight junctions (TJs) create ion-selective paracellular permeability barriers between extracellular compartments. In the organ of Corti of the inner ear, TJs of the reticular lamina separate K^+-rich endolymph and Na^+-rich perilymph. In humans, mutations of the gene encoding claudin 14 TJ protein cause profound deafness but the underlying pathogenesis is unknown. To explore the role of claudin 14 in the inner ear and in other tissues we created a mouse model by a targeted deletion of *Cldn14.* In the targeted allele a *lacZ* cassette is expressed under the *Cldn14* promoter. In *Cldn14-lacZ* heterozygous mice β-galactosidase activity was detected in cochlear inner and outer hair cells and supporting cells, in the collecting ducts of the kidney, and around the lobules of the liver. *Cldn14*-null mice have a normal endocochlear potential but are deaf due to rapid degeneration of cochlear outer hair cells, followed by slower degeneration of the inner hair cells, during the first 3 weeks of life. Monolayers of MDCK cells expressing claudin 14 show a 6-fold increase in the transepithelial electrical resistance by decreasing paracellular permeability for cations. In wild type mice, claudin 14 was immunolocalized at hair cell and supporting cell TJs. Our data suggest that the TJ complex at the apex of the reticular lamina requires claudin 14 as a cation-restrictive barrier to maintain the proper ionic composition of the fluid surrounding the basolateral surface of outer hair cells.

INTRODUCTION

A hallmark in the development of multicellular organisms is the separation of fluid compartments by sheets of epithelial cells, which adhere to each other by using different types of intercellular junctions (1). Movement of solutes and water through epithelia occurs both across and between cells, and is referred to as the transcellular and the paracellular routes, respectively. The major selective barrier of the paracellular pathway is created by tight junctions (TJs) (2,3). In freeze fracture replicas of epithelial cells, TJs appear as a band-like network of branching and interconnecting thin ridges or complementary grooves, known as TJ strands (4,5). TJ strands of adjacent cells associate laterally with each other (3), thus sealing the intercellular space and preventing or reducing paracellular diffusion (1). In addition to this barrier function

*To whom correspondence should be addressed at: 5 Research Court, Room 2A-19, NIDCD/NIH, Rockville, MD 20850, USA. Tel: +1 3014967882; Fax: +13014027580; Email: friedman@nidcd.nih.gov
[†]Present address:
Kansai Medical University, Department of Otolaryngology, 10–15 Fumizonocho, Moriguchi, Osaka 570–8507, Japan.

TJs contribute to the maintenance of cellular polarity by forming an intramembrane barrier that restricts the lateral diffusion of apical and basolateral epithelial membrane components, which is referred to as the 'fence function' (6–9).

TJ strands are composed of at least three types of membrane-spanning proteins: (i) occludin (10); (ii) members of the claudin family (11); and (iii) members of the junction adhesion molecule (JAM) family (12–14). Interactions of these membrane proteins with the actin-based cytoskeleton and with membrane-associated proteins are important for the structural organization of the junctional complex at the plasma membrane and for signal transduction (15–22).

The claudins are a family of more than 20 highly conserved TJ proteins which share the same membrane topology and have various tissue distribution patterns (23). Many tissues express several different claudins which can interact with each other in both homotypic and heterotypic manners (23,24). Selectivity and specificity of paired TJ strands are determined by the type of claudins present and their mixing ratios (11,25–27).

The importance of claudins in creating the physiological and structural paracellular barrier function of TJs is supported by the finding that *Clostridium perfringens* enterotoxin removes specific claudins from TJ strands in the intestinal epithelium, causing TJ disintegration and reduction of the TJ barrier function (28). Yet, some claudins are not restricted to TJs (29,30), and it was suggested that they might have additional roles in cell–cell adhesion and embryonic development (31,32).

Pathological phenotypes of humans and animals with mutations in specific claudin genes further demonstrate the importance of these TJ proteins. *CLDN16* mutations cause familial hypomagnesemia with hypercalciuria and nephrocalcinosis in humans (33) and chronic interstitial nephritis in cattle (34,35), both due to dysfunction of paracellular renal transport mechanisms. *Cldn11*-null mice demonstrate neurological and reproductive deficits, due to the absence of TJs in the central nervous system myelin and between Sertoli cells (36). *Cldn1*-null mice and transgenic mice overexpressing *Cldn6* die shortly after birth due to dysfunction of the epidermal permeability barrier (37,38). We reported that recessive mutations of human *CLDN14* cause profound, congenital deafness, thus demonstrating a necessary but unknown role of claudin 14 in the hearing process (39).

In the cochlea of the inner ear (Fig. 1A), the endolymph of the scala media has high K^+ and low Na^+ concentrations, as opposed to the perilymph of the scala vestibuli and scala tympani, which has high Na^+ and low K^+ concentrations, similar to cerebrospinal fluid (40,41). The apical membranes of outer hair cells (OHCs) are exposed to endolymph, whereas the extracellular space that surrounds the basolateral membranes of OHCs (the space of Nuel) (Fig. 1A) is filled with cortilymph, which is similar to perilymph in its composition (42,43). The transepithelial potential of 80–100 mV between the endolymphatic and the perilymphatic space, which is defined as the endocochlear potential (EP), is generated by cells in the stria vascularis (44–48). The EP is critical for maintaining the proper sound-induced changes of intracellular potential in sensory hair cells (49,50). Separation of perilymph and cortilymph from endolymph is achieved by TJs which seal the spaces between the cells bordering the compartments containing these fluids (51). We have previously hypothesized that claudin 14-related deafness is due to failure in maintaining fluid compartmentalization in the inner ear (39).

To explore the role of claudin 14 in the inner ear and in other organs we created *Cldn14*-null mice. The data suggests that the absence of claudin 14 from hair cell–supporting cell and supporting cell–supporting cell TJs leads to altered ionic permeability through the reticular lamina. This, in turn, triggers rapid degeneration of cochlear hair cells during the second and third weeks of life, when hearing function in mice is being established.

RESULTS

Generation of *Cldn14*$^{+/-}$ mice

Cldn14, the gene encoding claudin 14, has three exons, with the entire protein of 239 amino acid residues encoded in exon three (39). A targeting vector was constructed and used to replace exon three with the neomycin resistance gene and the *lacZ* reporter gene, by homologous recombination in R1 embryonic stem (ES) cells (52) (Fig. 1B). Two lines of mice were generated from distinct recombinant ES cell clones, in which one of the two wild type (wt) *Cldn14* alleles was disrupted (*Cldn14*$^{+/-}$) (Fig. 1C).

Cldn14 expression pattern

We used an important feature of the targeting strategy, which placed the *lacZ* reporter gene under control of the endogenous *Cldn14* promoter (Fig. 1B), to study *Cldn14* expression pattern in *Cldn14*$^{+/-}$ mice (Fig. 2). At postnatal day 0 (P0), β-galactosidase activity was detected by X-gal staining in OHCs at the basal turn of the cochlea (Fig. 2A–C). At P4 β-galactosidase activity was also found in inner hair cells (IHCs) and, to a lesser extent, in supporting cells, of the middle and apical turns (Fig. 2D–F). By P7 β-galactosidase activity was observed in IHCs, OHCs and supporting cells throughout the cochlea, from base to apex (Fig. 2G–I). Low β-galactosidase activity was observed in some spiral prominence cells adjacent to the stria vascularis and in the sensory epithelium of the vestibular system (data not shown). β-Galactosidase activity was also detected in the collecting ducts of the kidney and around the lobules in the liver of adult *Cldn14*$^{+/-}$ mice (Fig. 2Y and Z). The data obtained from the *lacZ* reporter gene, which reflects *Cldn14* expression, is in agreement with our previously reported findings, which were based on *in situ* hybridization, immunostaining and northern blot analysis (39).

Cldn14-null mice have profound hearing loss with normal vestibular function

Two clones of *Cldn14*$^{+/-}$ ES cells were used to generate two lines of *Cldn14*-null mice (*Cldn14*$^{-/-}$) on a C57BL/6 and (129X1/SvJ × 129S1/SvImJ) mixed background. Intercrossing of heterozygotes yielded *Cldn14*$^{-/-}$, *Cldn14*$^{+/-}$ and *Cldn14*$^{+/+}$ mice at the expected Mendelian ratio of 1 : 2 : 1 (80 : 179 : 83), respectively. Genotypes were confirmed by Southern blot analysis (Fig. 1C). No *Cldn14* transcripts were detected by reverse transcription (RT)–PCR from kidneys of *Cldn14*$^{-/-}$

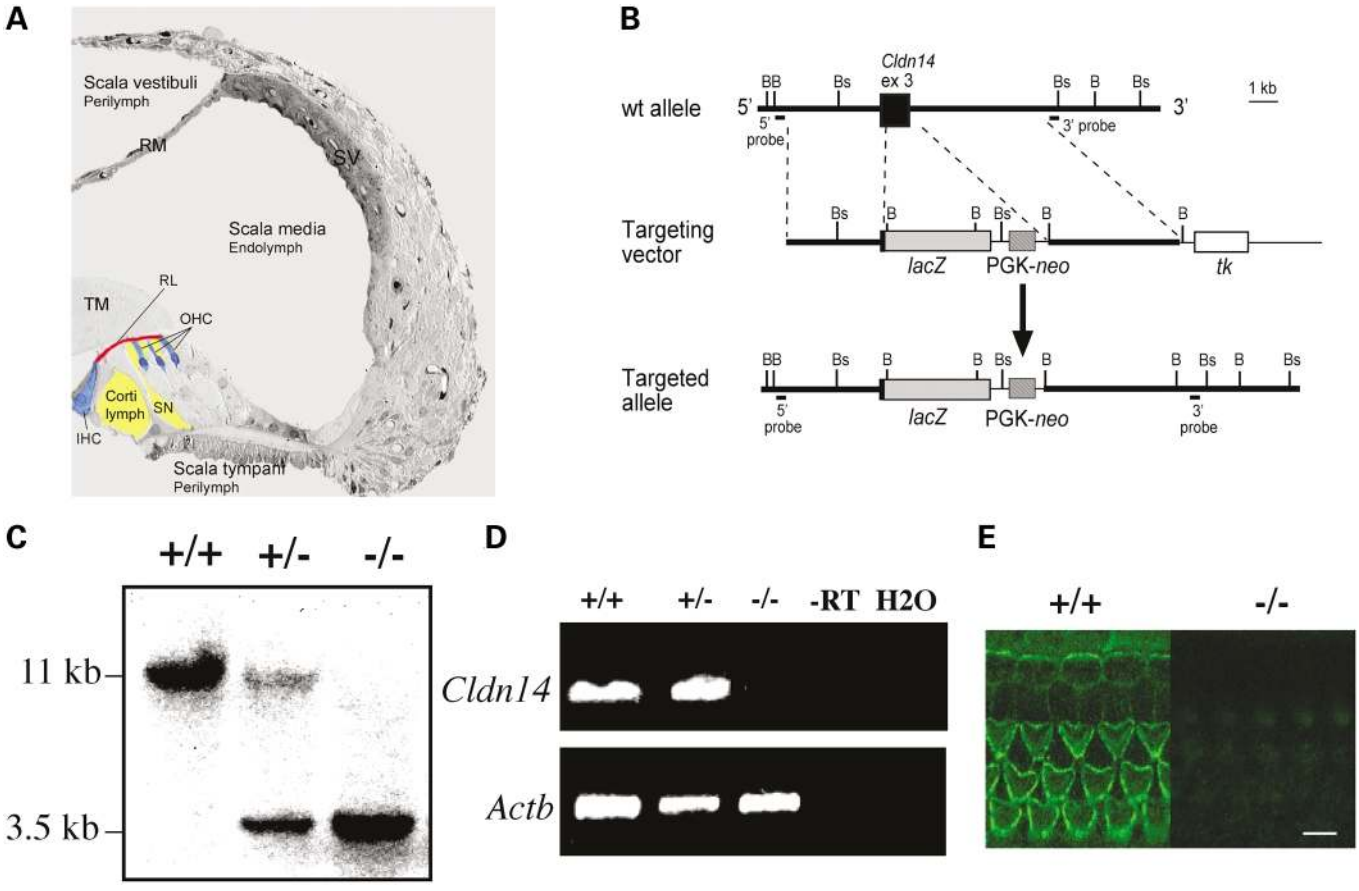

Figure 1. Generation of *Cldn14*-null mice. (**A**) A reconstructed image (40×) of a Lowicryl embedded section (1 μm thick) of freeze-substituted organ of Corti from a C57Bl/6 mouse at P12. Outer hair cells (OHC) and inner hair cells (IHC) are colored in blue, the reticular llamina (RL) is colored in red, and the space of Nuel (SN) is colored in yellow. RM, Reissner's membrane; SV, stria vascularis; TM, tectorial membrane. (**B**) Schematic representation of the 3′ region of the wt *Cldn14* allele, the targeting vector and the targeted *Cldn14* allele after homologous recombination. PGK, mouse phosphoglycerate kinase-1 promoter; *neo*, neomycin resistance cassette; *tk*, HSV thymidine kinase cassette. The positions of 5′ and 3′ probes used for Southern blot analyses and of restriction endonuclease sites are indicated. B, *Bam*HI; Bs, *Bsm*I. (**C**) Southern blot analysis of *Bam*HI-digested genomic DNA from wt (+/+), heterozygous (+/−) and *Cldn14*-null homozygous (−/−) mice using the 5′ probe reveals fragments of 11 kb and 3.5 kb from the wt and mutant alleles, respectively. (**D**) RT–PCR detection of *Cldn14* expression (660 bp product) in kidneys of wt (+/+) and heterozygotes (+/−), but not in *Cldn14*-null homozygous (−/−) mice. Similar amplification of β-actin (*Actb*) (465 bp product) demonstrates approximately equal amounts of mRNA in all samples. Also shown for each set of reactions are controls in which the cDNA template was substituted by water (H_2O) or by the product of a mock cDNA synthesis (−RT). (**E**) Whole-mount OC of a wt (+/+) and a *Cldn14*-null homozygous (−/−) mouse at P7 were processed for immunostaining with an anti-claudin 14 antibody (green). In the wt mouse claudin 14 was localized at the junctional complex along the most apical borders of IHCs, OHCs and supporting cells (also see Fig. 6A). No junctional staining was observed in the $Cldn14^{-/-}$ mouse. Scale bar = 6 μm.

mice (Fig. 1D) and no junctional staining was observed in sensory hair cells of $Cldn14^{-/-}$ mice stained with an anti-claudin 14 antibody (Fig. 1E). Data is presented for one of the two lines of mice, which had identical phenotypes.

$Cldn14^{-/-}$ mice are fertile and appear healthy. Histopathological examination of 41 tissues and a panel of chemistry tests of serum derived from $Cldn14^{-/-}$, $Cldn14^{+/-}$ and $Cldn14^{+/+}$ mice revealed no differences between mice of these three genotypes, including kidney and liver structure and function (data not shown). $Cldn14^{-/-}$ mice display no obvious abnormal behavior which might indicate vestibular dysfunction, such as circling, head tossing or hyperactivity. Based on rotarod and elevated beam testing (53,54) vestibular and motor functions of $Cldn14^{-/-}$ mice are indistinguishable from those of $Cldn14^{+/-}$ and $Cldn14^{+/+}$ mice (data not shown).

To evaluate hearing, $Cldn14^{-/-}$ and their heterozygous and wt littermates underwent auditory brainstem response (ABR) analyses. At 4 weeks of age $Cldn14^{-/-}$ mice were found to have a profound hearing loss, with ABR thresholds elevated by 50 dB-SPL or more over all frequencies tested, while thresholds of heterozygous and wt mice were indistinguishable from each other (Fig. 3). ABR analyses demonstrated that $Cldn14^{-/-}$ mice were already deaf by the third week of life (P15–P17) (data not shown). Hearing loss in $Cldn14^{-/-}$ mice was not caused by reduction or absence of EP, as indicated by normal EP values which were measured in $Cldn14^{-/-}$ mice at 5 and 10 weeks of age (data not shown).

OHCs and IHCs in inner ears of *Cldn14*-null mice degenerate during the second and third postnatal weeks

Scanning electron microscopy (SEM), immunohistochemistry and X-gal staining revealed that the inner ear of $Cldn14^{-/-}$ mice developed normally and both IHCs and OHCs were

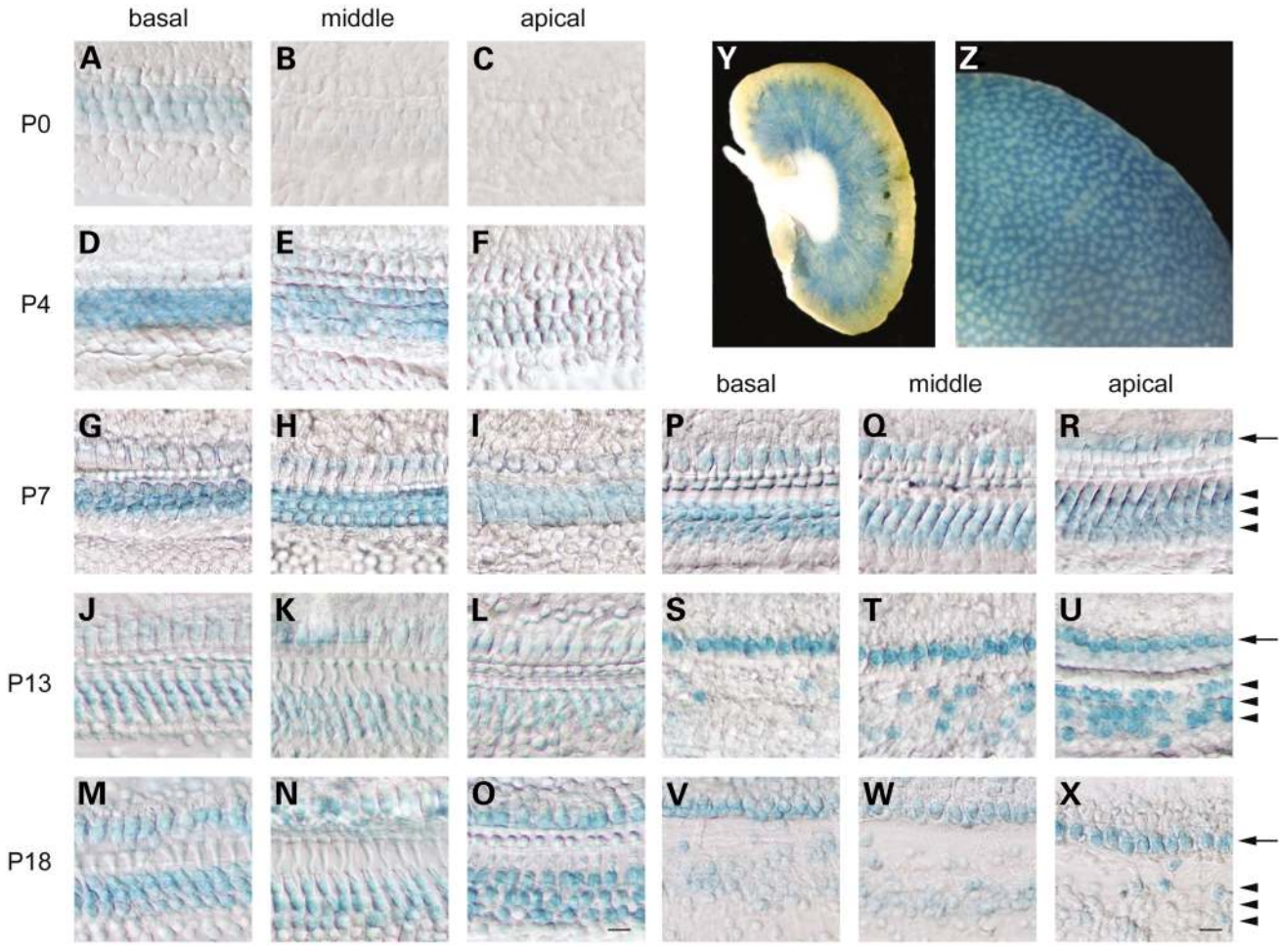

Figure 2. Whole-mount X-gal staining of the organ of Corti (OC), kidney and liver of *Cldn14*$^{+/-}$ and *Cldn14*$^{-/-}$ mice. Whole-mount X-gal staining for β-galactosidase activity in the OC of *Cldn14*$^{+/-}$ mice at P0 (**A**–**C**), P4 (**D**–**F**) and P7 (**G**–**I**) shows spreading of β-galactosidase activity in the three lines of OHCs (marked by arrowheads), the single line of IHCs (marked by an arrow) and in supporting cells, from base to apex. In *Cldn14*$^{-/-}$ mice both IHCs and OHCs are present and normally organized at P7 (**P**–**R**). At P13 OHCs are mostly missing at the base and partially missing at the middle and at the apex of the cochlea (**S**–**U**). By P18 most OHCs are missing throughout the cochlea (**V**–**X**). Similar degeneration of OHCs is not observed in the OC of age-matched *Cldn14*$^{+/-}$ mice (**J**–**O**). Whole-mount X-gal staining of kidney and liver of an adult *Cldn14*$^{+/-}$ mouse demonstrates β-galactosidase activity in the collecting ducts of the kidney (**Y**) and around the lobules in the liver (**Z**). No staining was observed in corresponding samples from wt mice. Scale bars = 10 μm.

present and undistinguishable from the wt at P7 (Figs 2P–R, 4B, 5G and J). However, subsequently rapid loss of OHCs was observed, which progressed from base to apex. At P10–P13 OHCs were missing or disorganized throughout most of the cochlear length of *Cldn14*$^{-/-}$ mice, except for the extreme apex (Figs 2S–U, 4E, 5H and K). By P18 only a few OHCs with disorganized stereocilia were present, mainly at the most apical region of the cochlea (Figs 2V–X, 5I and L). Throughout the cochlea IHCs were partially missing and some had abnormal stereocilia (Figs 2S, 5H and I).

In *Cldn14*$^{-/-}$ mice, the first sign of OHC degeneration was disorganization and loss of stereocilia, followed by swelling of cell bodies, shortening of the cell length and submerging of the cell bodies under the reticular lamina, where these cells eventually lost their integrity and died. For example, at P18 no OHC stereocilia were observed at the cochlear apex of *Cldn14*$^{-/-}$ mice by SEM (Fig. 4D). However, X-gal staining and immunocytochemistry with antiserum to prestin, an OHC-specific motor protein and the main constituent of their lateral plasma membrane (55), revealed that the cell bodies of some OHCs were still present, although several of them were degenerated (Fig. 5L).

Membrane-associated claudin 14 is restricted to TJs between cells of the reticular lamina of the mouse OC

To study claudin 14 cellular localization, we performed immunohistochemistry with an affinity-purified claudin 14 antibody. In inner ears of adult wt C57BL/6 mice immunoreactivity was detected at the junctional complex along the most apical borders of IHCs, OHCs and supporting cells (Fig. 6A–C) and in the cytoplasm of inner and outer pillar cells, Deiter's cells and to a lesser extent in the cytoplasm of IHCs and OHCs (Fig. 6D and E). No immunoreactivity was detected in TJs between the cells of Reisner's membrane, the stria vascularis or in the junctional complex of inner sulcus cells, outer sulcus cells, and

A

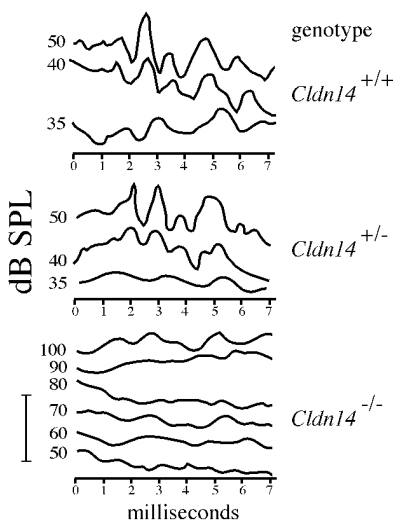

B

Genotype	Number of Ears Analyzed	Frequency (kHz) Click	8	16	32
Cldn14 $^{+/+}$	13	43±5	47±5	42±4	24±5
Cldn14 $^{+/-}$	19	41±4	47±4	37±6	22±6
Cldn14 $^{-/-}$	17	100±0 (5)	97±3 (11)	97±3 (3)	86±9 (14)
		>100 (12)	>100 (6)	>100 (14)	>100 (3)

Figure 3. ABR analyses of *Cldn14*$^{+/+}$, *Cldn14*$^{+/-}$ and *Cldn14*$^{-/-}$ mice. (**A**) Shown is a sample ABR analysis for a click stimulus from a 4-week-old *Cldn14*$^{-/-}$ mouse and his *Cldn14*$^{+/-}$ and *Cldn14*$^{+/+}$ littermates. The horizontal axis is time in milliseconds; the vertical axis is sound intensity in dB-SPL. The bar to the left of the recordings is a normalized scale of 3 mV. Observed thresholds in this sample were 40 dB-SPL for the *Cldn14*$^{+/+}$ and *Cldn14*$^{+/-}$ mice, and >100 dB-SPL for the *Cldn14*$^{-/-}$ mouse. (**B**) Mean ABR thresholds (dB-SPL) of *Cldn14*$^{+/+}$, *Cldn14*$^{+/-}$ and *Cldn14*$^{-/-}$ mice. Results for *Cldn14*$^{-/-}$ mice are divided into two groups: for ears with ABR thresholds ≤100 dB-SPL the mean thresholds were calculated. Other ears did not have a threshold at 100 dB-SPL, which is the maximum sound intensity tested for each frequency. The number of ears included in each of these two groups is indicated in brackets.

spiral prominence cells (data not shown). A similar pattern of immunoreactivity was observed in the inner ear of wt mice at P7 (Fig. 1E). In inner ears of *Cldn14*$^{-/-}$ mice at P7 only some cytoplasmic staining in supporting cells was observed, which is probably non-specific. No junctional staining was observed in *Cldn14*$^{-/-}$ mice, further validating the specificity of the antibody against claudin 14 (Fig. 1E). These observations indicate that membrane-associated claudin 14 is restricted to TJs between cells of the reticular lamina of the mouse OC.

Freeze fracture replicas reveal normally appearing TJ strands between OHCs and supporting cells in the OC of *Cldn14*-null mice

We used transmission electron microscopy of freeze fracture replicas to observe the morphology of TJ strands between OHCs and supporting cells in the OC of *Cldn14*$^{-/-}$ mice at P7, before the loss of OHCs occurs. No obvious qualitative or quantitative differences were observed between TJ strands of *Cldn14*$^{-/-}$ and *Cldn14*$^{+/+}$ mice (Fig. 6F and G).

OHCs of OC explants of *Cldn14*$^{-/-}$, *Cldn14*$^{+/-}$ and *Cldn14*$^{+/+}$ mice survive equally well under normal culture conditions

To determine whether degeneration of OHCs of *Cldn14*$^{-/-}$ mice is triggered by a signal intrinsic to the cell or by extracellular conditions, we maintained for up to 10 days (from P3–P5 to P10–P14) explants derived from the middle turn of the OC of *Cldn14*$^{-/-}$, *Cldn14*$^{+/-}$ and *Cldn14*$^{+/+}$ mice in DMEM culture medium containing 5.3 mM of K^+. Explants were fixed at P10 and at P14 and immunostained with the anti-prestin antibody, which revealed that in OC explants of *Cldn14*$^{-/-}$ mice OHCs survived as well as in OC explants of *Cldn14*$^{+/-}$ and *Cldn14*$^{+/+}$ mice, and only a few OHCs were missing in all cases (Fig. 7A and B). This is in contrast to OC of *Cldn14*$^{-/-}$ mice *in vivo*, in which by P10 (Fig. 4E) and P13 (Figs 7C and 2T) most of the OHCs of the middle turn of the cochlea were missing. By P13 *in vivo* OHCs were partially missing from the apical turn as well (Figs 2U, 5H and K).

Claudin 14 expressed in cultured epithelial monolayers increases paracellular resistance through a selective discrimination against cations

We next asked whether claudin 14 confers electrophysiologic properties to TJs that are consistent with its proposed role in maintaining the paracellular ion barrier at the reticular lamina. As we have published for claudins 2, 4 and 15, claudin 14 was expressed under a tightly inducible promoter in cultured clonal monolayers of MDCK II cells, the cells were grown on porous culture inserts and the relevant paracellular properties directly measured using an Ussing-type chamber (27,56). Prior to induction we detect no claudin 14 by immunoblotting (Fig. 8A) or by indirect immunofluorescence microscopy. After removal of doxycycline from the growth media for 4 days strong immunoblot and immunolocalization signals are observed, with localization at the TJ (Fig. 8A and data not shown). Expression of claudin 14 coincides with a 6-fold increase in the transmonolayer electrical resistance (TER) (Fig. 8B). The dilution potentials for NaCl reveal a reversal, which occurs because the permeability ratio for Na^+ to Cl^- (P_{Na}/P_{Cl}) is strongly decreased. This change in ionic permeability ratio is completely explained by a strong discrimination against Na^+ without any change in Cl^- permeability. Bi-ionic dilution potentials revealed a similar relative discrimination against all the alkali metal cations, without a change in their relative permeability ($K^+ > Na^+ > Rb^+ > Li^+ > Cs^+$) (data not shown). We conclude that claudin 14 incorporates into TJs and strongly discriminates against paracellular movement of cations.

DISCUSSION

The importance of claudin 14 for normal hearing was demonstrated by the association between profound congenital deafness and mutations of *CLDN14* (39). The phenotype of *Cldn14*-null mice is similar to the human phenotype: homozygotes for the null allele have profound hearing loss, with normal vestibular

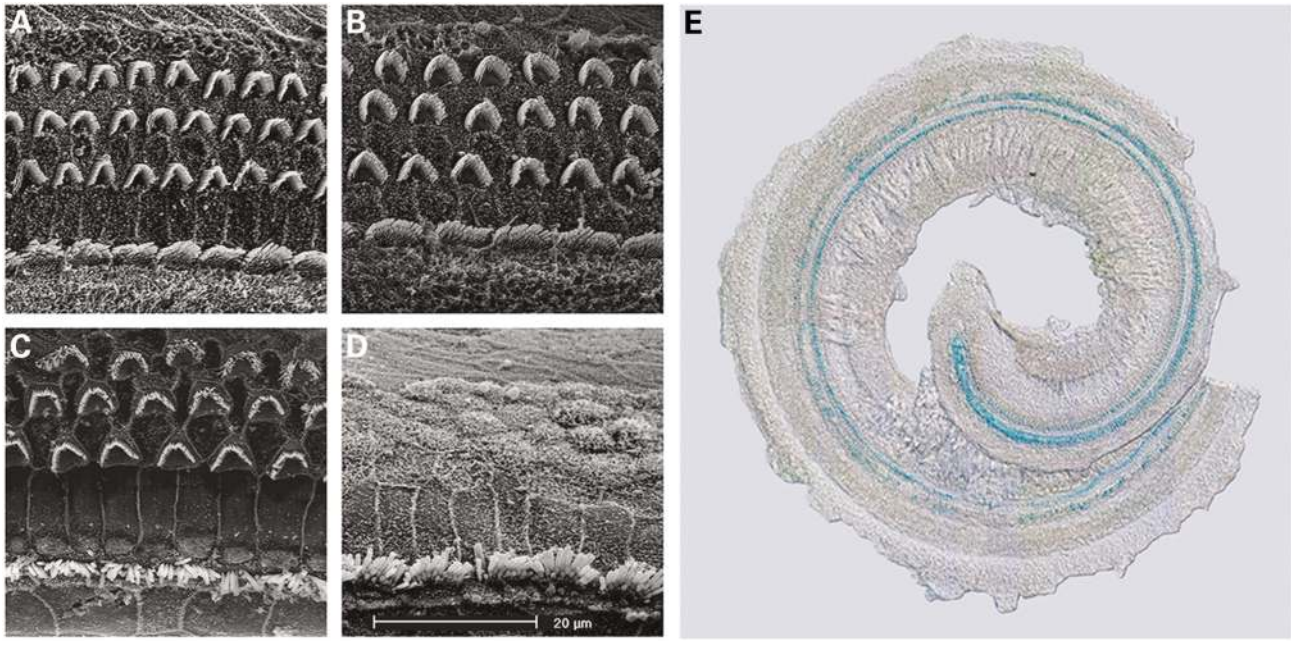

Figure 4. Hair cell degeneration in the organ of Corti (OC) of *Cldn14*$^{-/-}$ mice. Scanning electron microscopy (SEM) micrographs of the organ of Corti reveal normally organized IHCs and OHCs at P7 in both *Cldn14*$^{+/+}$ (**A**) and *Cldn14*$^{-/-}$ mice (**B**). By P18 IHCs and OHCs appear normal in *Cldn14*$^{+/+}$ mice (**C**) but stereocilia of OHCs are completely missing in *Cldn14*$^{-/-}$ mice (**D**). Scale bar = 20 µm. (**E**) A reconstructed image (20×) of whole-mount OC from the apical turn of the cochlea of a *Cldn14*$^{-/-}$ mouse at P10, following X-gal staining, shows base-to-apex progression of OHC degeneration.

function, while heterozygotes have normal hearing (Fig. 3). In addition to the OC, *Cldn14* is expressed in the sensory epithelium of the vestibular system, and in kidney and liver (Fig. 2Y and Z). Yet no renal, hepatic or vestibular dysfunction were observed in humans homozygous for *CLDN14* mutations (39), or in *Cldn14*-null mice, suggesting that in these tissues other claudins substitute for the function normally performed by claudin 14. Indeed, in the tissues expressing *Cldn14*, other claudin genes are expressed as well (23,36,57–60). While claudin 14 is indispensable in the inner ear, it does not seem to be necessary for normal kidney and liver functions. These observations demonstrate that TJ strands in certain tissues contain multiple claudins, some of which are indispensable, while others appear to be functionally redundant.

In mammals, OHCs are electromechanical cochlear amplifiers which enhance hearing sensitivity by more than 40 dB (61,62). This function of OHCs is mediated by the tectorial membrane. A targeted deletion of the mouse *Tecta* gene, encoding α-tectorin, led to detachment of the tectorial membrane from the cochlear epithelium, and reduced hearing sensitivity by 35 dB–SPL (63). A hearing loss of 45–65 dB-SPL was observed in *prestin*-null mice, in which OHCs are present in most of the cochlea, but lack electromotility, and both OHCs and IHCs are missing from the basal 25% of the cochlear spiral (64). In *Cldn14*-null mice by the age of 3 weeks nearly all OHCs are lost, while there is only a partial loss of IHCs, which in combination lead to a hearing loss of 50–60 dB-SPL (Fig. 3).

In *Cldn14*-null mice TJ strands between supporting cells and between OHCs and supporting cells in the OC are still present and appear morphologically normal in freeze fracture replicas (Fig. 6F and G), suggesting that these TJs contain other claudins in addition to claudin 14. A similar observation was made in *Cldn1*-null mice, where TJ strands in the epidermis were not affected morphologically, but nevertheless failed to maintain the epidermal permeability barrier (37). These findings demonstrate that the elimination of an essential claudin from TJ strands which are composed of multiple claudins may have a functional, but not necessarily an ultrastructural effect that could be detected by electron microscopy. In contrast, in *Cldn11*-null mice there is a complete absence of TJ strands from the central nervous system myelin and between Sertoli cells (36), suggesting that claudin 11 is either the only claudin in these TJs, or that it is essential for TJ formation and/or maintenance.

One of the roles of TJs in epithelial physiology is maintenance of cellular polarity (6). The intact TJ strands between OHCs and supporting cells in the OC of *Cldn14*$^{-/-}$ mice observed by freeze fracture replicas (Fig. 6F) seems to exclude a selective breakdown of apical membrane polarization. During OHC degeneration in *Cldn14*$^{-/-}$ mice, the cuticular plate, an actin-rich region found at the apical end of OHCs, was present even after stereocilia were lost and OHC bodies descended under the reticular lamina, and the localization of prestin to the lateral membrane of OHCs was not affected (Fig. 5J–L). These findings suggest that loss of cell polarity may not be the cause for OHC death in *Cldn14*$^{-/-}$ mice, which maintain at least some aspects of cell polarity. However, the possibility of partially altered cell polarity as a cause for OHC degeneration in *Cldn14*$^{-/-}$ mice cannot be ruled out.

TJ transmembrane proteins have been shown to be involved in signal transduction pathways (65) through their interactions with other membrane-associated proteins, such as ZO-1, ZO-2, ZO-3 (66) and MUPP1 (19). Some of these proteins, in turn, are implicated in signal transduction pathways that regulate

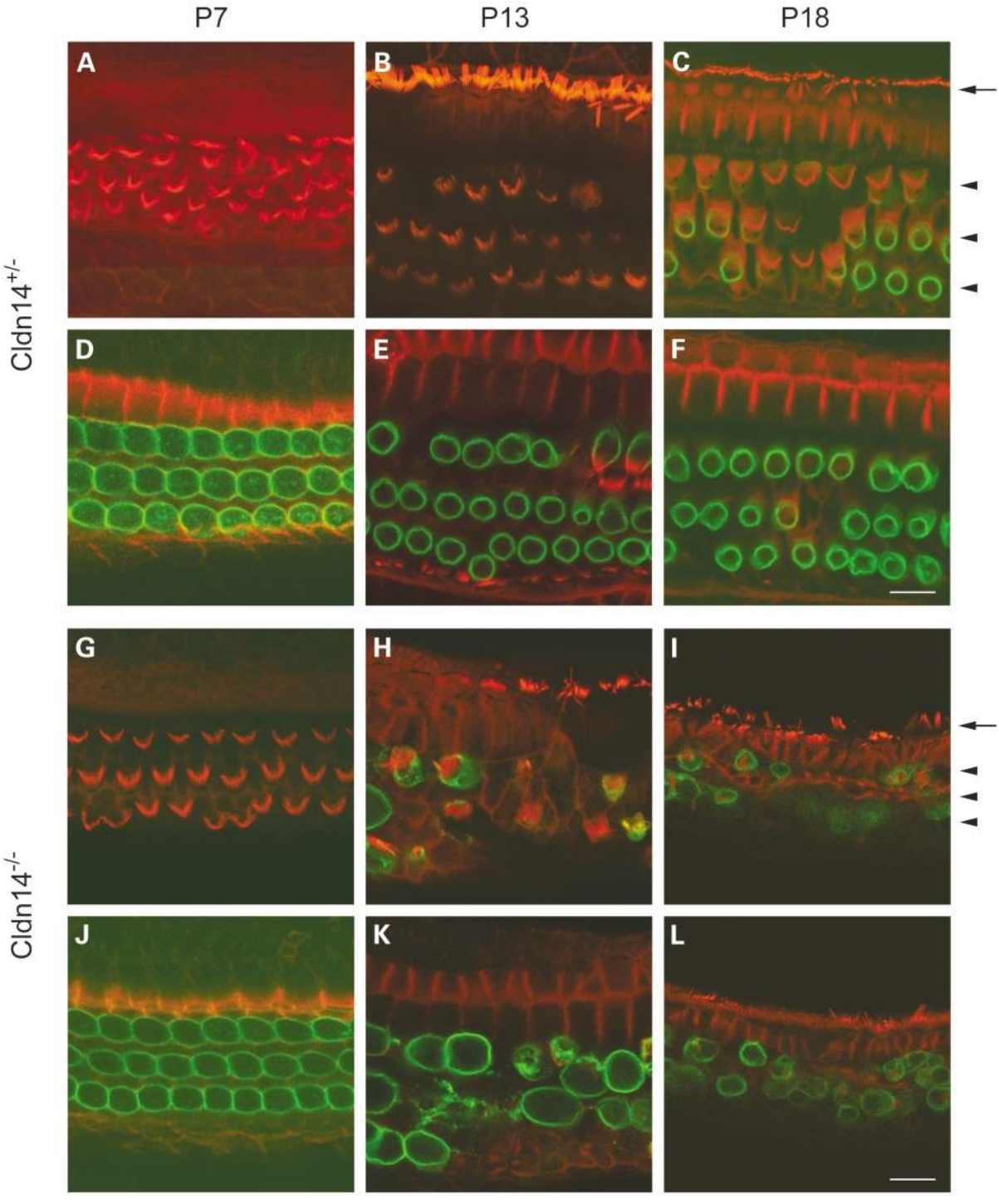

Figure 5. Immunohistochemistry of the organ of Corti (OC) of *Cldn14*$^{+/-}$ and *Cldn14*$^{-/-}$ mice with an anti-prestin antibody and rhodamine-phalloidin. Whole-mount OC of *Cldn14*$^{+/-}$ and *Cldn14*$^{-/-}$ mice at P7, P13 and P18 were processed for immunostaining with an anti-prestin antibody (green), which served as a marker for OHC bodies. Rhodamine-phalloidin staining (red) was used to observe the actin-rich stereocilia and cuticular plate of cochlear hair cells. Shown are confocal cross-sections (0.6 µm thick) from the apical region, taken at the levels of the stereocilia (**A**–**C**, **G**–**I**) and the OHC body (**D**–**F**, **J**–**L**). Scale bar = 10 µm.

specific gene expression (67,68). Claudin 14-binding proteins and the signaling pathways in which claudin 14 is involved are unknown. The effect of the absence of claudin 14 on OHCs may result from altered expression of other genes which are required for OHC maintenance and survival. However, our experiments with OC explants argue against this hypothesis. OHCs of OC explants of *Cldn14*$^{-/-}$ mice survived as well as those of *Cldn14*$^{+/+}$ mice up to P14, after 10 days in normal culture conditions. In contrast, most OHCs of the middle turn of OC of *Cldn14*$^{-/-}$ mice *in vivo* are missing by P10, and by

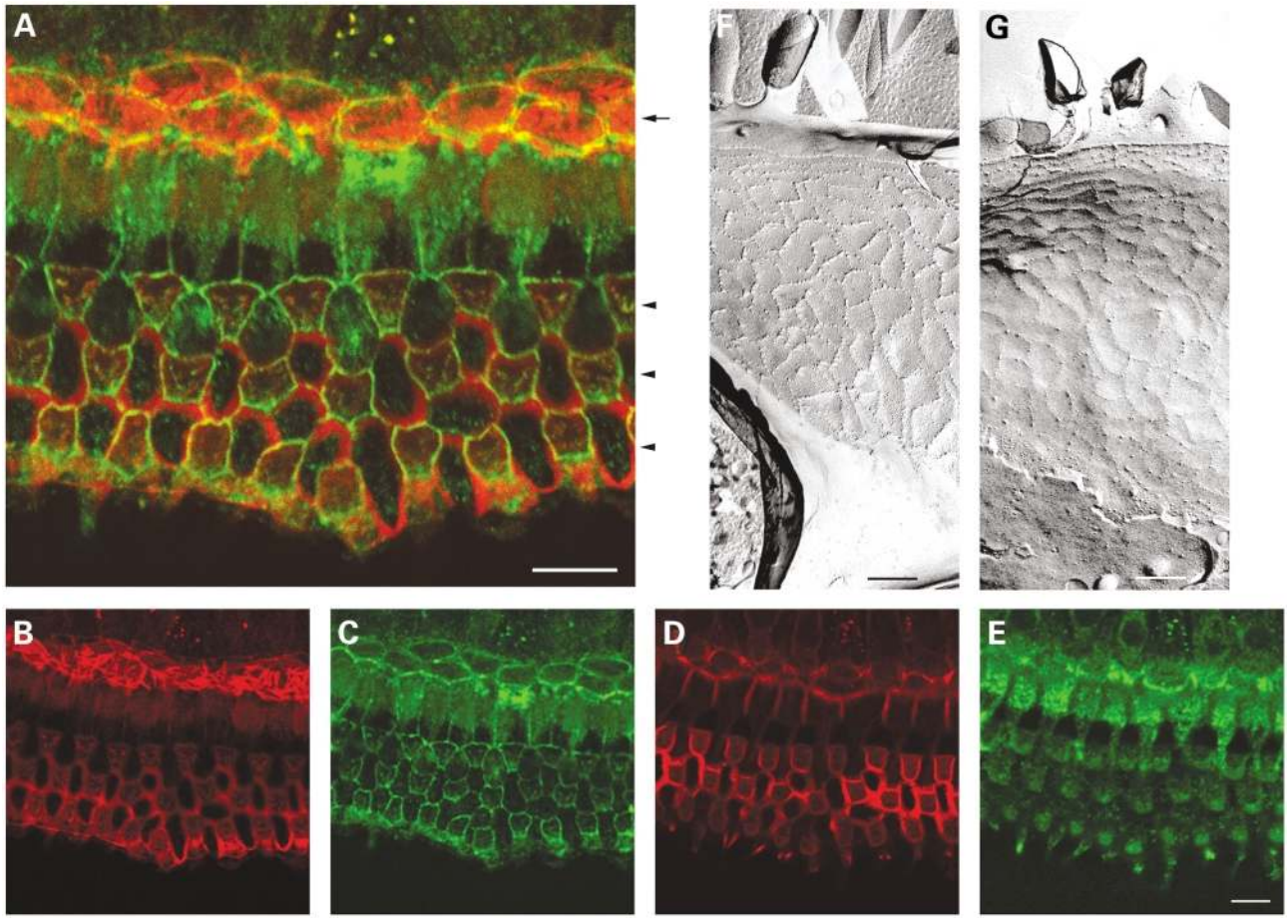

Figure 6. Immunolocalization of claudin 14 in the mouse organ of Corti (OC) and freeze fracture replicas of the apical junctional region of OHCs in the OC of *Cldn14*$^{-/-}$ and *Cldn14*$^{+/+}$ mice. (**A**–**E**) Whole-mount OC of an adult C57B1/6 mouse was processed for immunostaining with an anti-claudin 14 antibody (green). Rhodamine-phalloidin staining (red) was used to observe the actin-rich stereocilia and the cuticular plate of cochlear hair cells. Shown are confocal cross-sections of the reticular lamina (0.7 µm thick) taken at different focal planes. (A) The double immunostaining of the optical section of the outermost layer of the reticular lamina. Claudin 14 was localized at the junctional complex along the most apical borders of IHCs, OHCs and supporting cells. The single row of IHCs is marked by an arrow. The three rows of OHCs are marked by arrowheads. No junctional staining was observed in *Cldn14*$^{-/-}$ mice, further validating the specificity of the antibody against claudin 14 (Fig. 1E). (B and C) The red and green channels, respectively, of the same focal plane of the OC, stained with rhodamine-phalloidin (B) and with the anti-claudin 14 antibody (C). Note the bright outlines of the junctions between the heart-shaped cuticular plates of the OHCs, oval-shaped cuticular plates of the IHCs and apical surfaces of the supporting cells stained with the anti-claudin 14 antibody. (D and E) Represent the red (D) and green (E) channels, respectively, of the optical section 2 µm below the optical sections depicted in (B and C), but still at the level of OHC cuticular plates. No staining with anti-claudin 14 antibody is observed at this optical section level along the junctions between hair cells and supporting cells, but cytoplasmic staining in the OHCs, IHCs and supporting cells is seen (E). Scale bar = 10 µm. (**F** and **G**) Freeze fracture replicas of the p-face of OHC apical junctional region in the OC of *Cldn14*$^{-/-}$ (F) and *Cldn14*$^{+/+}$ (G) mice at P7.TJ strands appear as several rows of particles (ridges) which are parallel to the apical membrane (top) and a complex pattern of ridges running basally (bottom). The smooth face above the parallel TJ strands is the p-face of the OHC apical membrane. Scale bar = 200 nm.

P13 many OHCs are missing from the apical turn as well. This observation suggests that OHC death in *Cldn14*$^{-/-}$ mice is not triggered by a signal intrinsic to the cell, but by extracellular factors.

TJs play a central role in regulation of paracellular permeability (1). It has been hypothesized that claudins create charge-selective channels in the paracellular space and that paracellular ionic selectivities of different epithelia are determined by varying combinations and levels of different claudins. Moreover, it was suggested that claudins determine ion permeability through the electrostatic charges on their extracellular amino acid residues (56). For example, discrimination against sodium ions by claudin 4 depended on a single basic residue in the first extracellular domain, while two of the three acidic residues in the first extracellular domain of claudin 15 were shown to affect discrimination against chloride ions (56). Following this line of reasoning, the first extracellular domain of claudin 14 contains eight basic residues (H29, R31, R32, H35, K48, H57, R68 and R81) (GenBank accession number AY029237), suggesting that it may be a barrier to positively charged ions, such as potassium.

We tested the electrophysiologic properties of claudin 14 by expressing it in cultured monolayers of MDCK cells under an inducible promoter. MDCK type II cells express many different claudins but the full pattern is not known for lack of reagents. However, *Cldn14* is not normally expressed in these cells (Fig. 8A). MDCK II monolayers are normally quite leaky (their paracellular conductance greatly exceeds transcellular

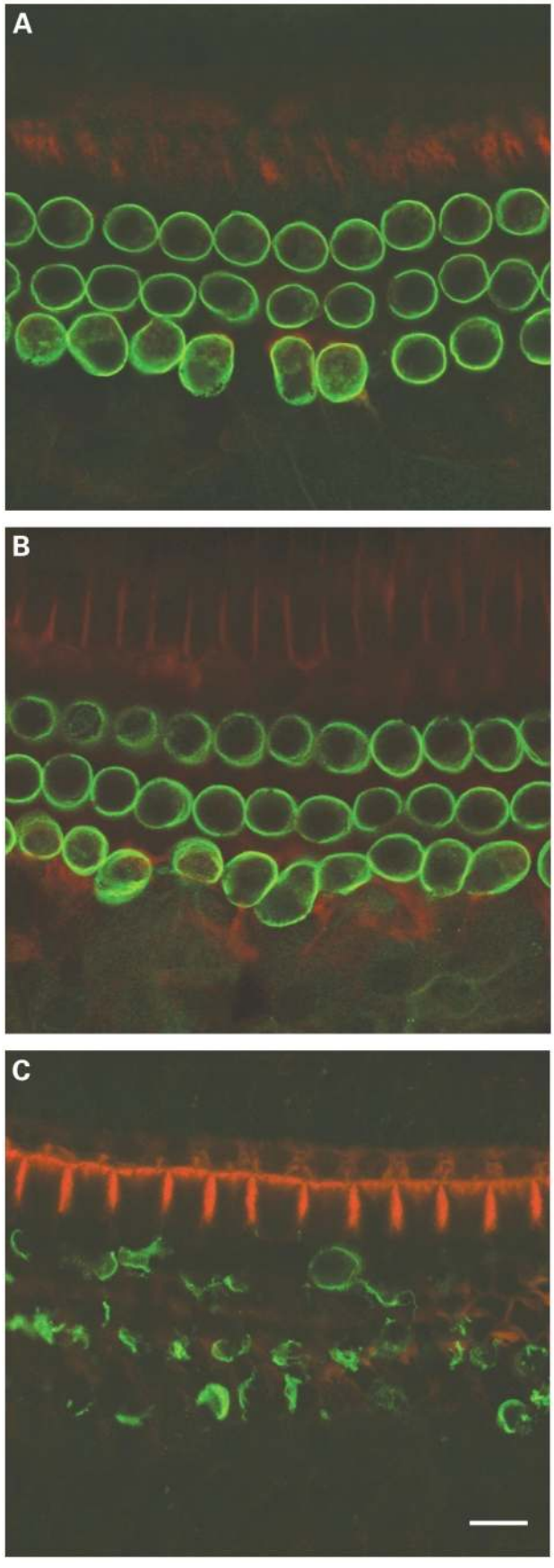

conductance). In addition, they are highly cation selective, as indicated by a P_{Na}/P_{Cl} value of 2.5 (27). Following expression of either claudin 4, claudin 14 or claudin 15 in MDCK II cells the monolayers become much tighter, as indicated by the increase in TER (27,56) (Fig. 8B). However, each one of these claudins has a different effect on selective ion permeability. Expression of claudin 15 does not significantly affect the normal Na^+ selectivity (56). Expression of claudin 4 decreases the P_{Na}/P_{Cl} value from 2.5 to 1.6, thus indicating a selective decrease in Na^+ permeability (27). Following expression of claudin 14 the ionic selectivity is reversed, indicating a strong discrimination against Na^+ and K^+ (Fig. 8B). These properties are precisely what would be required to maintain the high cation gradients between perilymph and endolymph. Presumably in the *Cldn14*-null mice and humans other claudins remain but lack the ability to maintain the paracellular barrier against cations at the reticular lamina.

The onset of OHC loss in *Cldn14*-null mice, at 8–9 days after birth, coincides with several important developmental processes which occur in inner ears of normal mice, including increase in endolymph K^+ concentration, onset of EP, and formation of the space between OHCs, which is referred to as the space of Nuel (69,70) (Fig. 1A). We hypothesize that the absence of claudin 14 from TJs in the OC leads to altered ionic permeability of the paracellular barrier of the reticular lamina (71), and perhaps results in elevated K^+ concentration in the space of Nuel, which is normally filled with the K^+-poor cortilymph (42,43). Long term exposure of the basolateral membranes of OHCs to high K^+ concentrations is toxic and causes prolonged OHC depolarization, which eventually leads to cell death (72,73). Our hypothesis regarding the cause for OHC loss in *Cldn14*-null mice is supported by our experiments with MDCK II monolayers transfected with *CLDN14* and with OC explants. A mechanism of OHC death due to K^+-intoxication was suggested to underlie the phenotype of mice deficient for the K-Cl co-transporter Kcc4, which are deaf due to early hair cell degeneration, explained by insufficient removal of K^+ from the space of Nuel (74). A similar mechanism of OHC degeneration was also suggested for hearing loss due to acoustic trauma (42,75).

Both IHCs and OHCs express similar levels of *Cldn14* (Fig. 2), but in contrast to OHCs, IHCs are less affected by the lack of claudin 14 (Figs 2, 4 and 5). IHCs may express additional claudins, which are not expressed in OHCs, and which compensate for the lack of claudin 14. In addition, unlike OHCs, the basolateral membranes of IHCs are not surrounded by a liquid-filled space. IHCs may be less sensitive than OHCs to an elevated concentration of K^+ or another factor which is causing OHC death in the absence of claudin 14.

Figure 7. OHCs of OC explants of *Cldn14*$^{-/-}$ and *Cldn14*$^{+/+}$ mice and of *Cldn14*$^{-/-}$ mice *in vivo.* OC explants from the middle turn of the cochlea were maintained in normal culture conditions from P4 to P14. At P14 explants were fixed and processed for immunocytochemistry using the anti-prestin antibody (green) and rhodamine-phalloidin (red), to observe OHC bodies and stereocilia, respectively. OHCs in OC explants of *Cldn14*$^{-/-}$ mice (**B**) survived as well as in OC explants of *Cldn14*$^{+/+}$ mice (**A**). This is in contrast to OC of *Cldn14*$^{-/-}$ mice *in vivo*, in which by P13 most of the OHCs of the middle turn of the cochlea were missing (**C**). Scale bar = 10 µm.

A

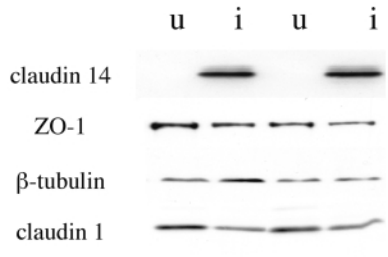

B

	Uninduced cells (+dox)	Induced cells (-dox)
ΔV_T (mV)[A]	7.28±0.47	-2.42±0.26*
TER (Ωxcm^2)	52.7±2.6	293.0±34.8*
P_{Cl}/P_{Na}[B]	0.373±0.29	1.37±0.47*
P_{Na} (10^{-6} cm/sec)[C]	28.03±1.11	7.7±0.76*
P_{Cl} (10^{-6} cm/sec)[C]	10.37±0.51	10.7±1.45*

Figure 8. Claudin 14 expressed in cultured epithelial monolayers increases paracellular resistance through a selective discrimination against cations. (**A**) Western blot analysis of two separate stable MDCK II Tet-Off cell lines transfected with *CLDN14*. Cells were cultured on filters for 4 days, uninduced (u) or induced (i) for transgene expression. Multiple aliquots of whole cell lysates were separated by SDS-PAGE, followed by immunoblotting with specific antibodies for claudin 14, ZO-1, β-tubulin and claudin 1. Endogenous claudin 14 was not detected in the uninduced cells. In the induced cells, a specific band of 26 kDa was detected by the claudin 14 antibody. (**B**) Mean ± STD error of three separate MDCK clones expressing *CLDN14*. Each measurement was determined in duplicate. [A]Dilution potential, corrected for electrode potential. [B]Calculated from the constant field equation. [C]Calculated using the Kimizuka–Koketzu equation. *$P < 0.0001$.

The normal EP values found in adult *Cldn14*-null mice indicate that function of the stria vascularis in these mice is normal. Considering the predicted failure in cochlear fluid compartmentalization in *Cldn14*-null mice, there are two possible explanations for this finding. The volume of liquid within the space of Nuel is very small relative to the scala media (Fig. 1A). Leakage of endolymph into this space may significantly change its ionic composition and cause OHC death. However, the effect of this leakage in the scala media may be undetectable, or it can be compensated for by increased K^+ secretion by the marginal cells of the stria vascularis (44,46). Alternatively, it is possible that the EP declines during the second and third weeks of life of *Cldn14*-null mice, while OHC loss is in progress. The reticular lamina might then be re-sealed by supporting cells, using TJs that do not include claudin 14, and thus by the age of 5 weeks the leakage of endolymph is minimized or stopped, and EP is restored.

In the OC the apical parts of hair cells and supporting cells form the reticular lamina, which maintains the ion barrier between endolymph and perilymph. This barrier is necessary for normal hearing (71). Occasional loss of hair cells occurs under normal conditions, while more pronounced OHC loss is observed after aminoglycoside treatment or noise trauma. Under these conditions the integrity of the reticular lamina is preserved by supporting cells, which provide a mechanism for maintenance of inner ear permeability barriers during structural reorganization (76–78). In *Cldn14*-null mice the absence of claudin 14 from TJs in the reticular lamina leads to rapid and massive death of OHCs, which provides insight into the pathogenesis of human deafness due to *CLDN14* mutations, and further demonstrates the important role of claudins in regulating the paracellular barrier.

MATERIALS AND METHODS

Cldn14 gene disruption

A 13 kb clone containing *Cldn14* exon three and flanking sequences was isolated from a 129X1/SvJ mouse genomic library (Stratagene, La Jolla, CA), and used to construct the targeting vector (Fig. 1B). A 3.3 kb DNA fragment from the second intron of *Cldn14* and including exon three splice-acceptor site was generated by PCR, using the following primers: 5′-AGGGACATGAAGGTAGAGGCTG-3′ and 5′-GCAGCTA-GCTTGACCAGTCGACCAGGGATGGATCTGGTCCTTAG-3′. This fragment was ligated to a 3.6 kb fragment harboring the *Escherichia coli lacZ* gene with a translation initiation codon in a Kozak consensus (CCACCatgG), and inserted into the *Xho* I site of the pPNT plasmid (79). A 4.7 kb DNA fragment derived from the region downstream of *Cldn14* exon three was generated by PCR, using the following primers: 5′-TG-ACCAGGATCCGAAAGCCTCATCTGAGTCCTGG-3′ and 5′-TGACCAGGATCCGCTCTAGTCCTGAAGAGTGAGC-3′. This fragment was inserted into the *Bam*HI site of pPNT. The PGK-*neo* cassette was located between the two fragments. For negative selection with Ganciclovir the HSV-*tk* cassette was placed downstream of the 3′ fragment of homologous sequence. The targeting vector was designed to replace exon three with PGK-*neo*, for positive selection with G418, and with the *lacZ* reporter gene, which would be transcriptionally regulated by the endogenous *Cldn14* promoter (Fig. 1B).

R1 ES cells (52) were electrophorated with the *Not* I-linearized targeting vector and grown in the presence of G418 and Ganciclovir, using standard protocols at the University of Michigan Transgenic Animal Model Core. A total of 384 resistant ES clones were screened for the homologous recombination event by Southern blot analysis with probes located both 5′ and 3′ to the integration site (Fig. 1B). Twelve recombinant clones were identified, and three of them were used for injection into C57BL/6 blastocysts, to generate chimeric mice. Mice heterozygous for the targeted allele were obtained by mating male chimeras with C57BL/6 females. Germline transmission was confirmed by Southern blot and PCR analyses. Animal experiments were performed according to the guidelines of the University of Michigan and the National Institute on Deafness and other Communication Disorders (NIDCD) Animal Care and Use Committee (ACUC) (protocol 971-00).

DNA and RNA analyses

Extraction of genomic DNA from mouse tails and Southern blot analysis were performed following standard procedures (80,81). Poly $(A)^+$ RNA was isolated from mouse kidney using Poly (A) Pure mRNA purification reagents (Ambion, Austin, TX). Reverse transcription was performed with 500 ng of

poly $(A)^+$ RNA in a 20 µl reaction volume using the Superscript first-strand synthesis system (Invitrogen, Carlsbad, CA). RT–PCR was performed with 2–4 µl of cDNA in a 50 µl reaction volume in the presence of 1× PCR reaction buffer (PE Applied Biosystems, Foster City, CA), 0.02 U of thermostable DNA polymerase, 10 pmol each of forward and reverse primers, 160 µM of each dNTP and 1.5 mM $MgCl_2$. Primer sequences were: *Cldn14* (GenBank accession number AY029237): 5′-CCAGCACAGCGGTCCAG-3′ and 5′-GGGGCACGGTTGTCCTTGTAG-3′; *Actb* (GenBank accession number NM_007393): 5′-GTCCACACCCGCCACCAGTTC-3′ and 5′-CCAGAGGCATACAGGGACAGC-3′. Cycling conditions were 95°C for 5 min, followed by 35 cycles of 95°C for 30 s, 60°C (*Cldn14*) or 57°C (*Actb*) for 30 s, and 72°C for 60 s (*Cldn14*) or 30 s (*Actb*), and a final step of 72°C for 10 min.

Histology

The following tissues were obtained from three males and three females of each genotype (*Cldn14*$^{-/-}$, *Cldn14*$^{+/-}$ and *Cldn14*$^{+/+}$) at the age of 4 weeks: brain, thymus, spleen, pancreas, lymph nodes, liver, kidneys, adrenal gland, salivary glands, Harderian gland, trachea, thyroid, esophagus, aorta, lung, testes, epididymis, urinary bladder, ovaries, uterus, oviducts, cervix, urinary bladder, prostate, seminal vesicles, preputial gland, heart, tongue, skeletal muscle, sciatic nerve, eyes, stomach, small intestine, cecum, colon, rectum, skin, sternum, vertebrae, femur and spinal cord. Tissues were fixed in buffered aqueous zinc formalin, embedded in paraffin, sectioned at 5 µm, and stained with hematoxylin and eosin (HE). Tissue samples containing bone were decalcified in a solution of formic acid and sodium citrate prior to sectioning.

Serum chemical analysis

Serum derived from six mice of each genotype (*Cldn14*$^{-/-}$, *Cldn14*$^{+/-}$ and *Cldn14*$^{+/+}$) at 4 weeks of age was analyzed by the Department of Laboratory Medicine at NIH (http://www.cc.nih.gov/cp/CC/animal/animal_test_menu.html). The analysis included complete serum chemistries and electrolytes, liver function tests, creatine kinase, GGTP, amylase, lipase, cholesterol, triglycerides and uric acid.

Auditory and vestibular testing

Vestibular function of 10 mice of each genotype (*Cldn14*$^{-/-}$, *Cldn14*$^{+/-}$ and *Cldn14*$^{+/+}$) was evaluated at 3 months of age by a rotarod test, with an accelerating speed treadmill (Stoelting, Wood Dale, IL), and by a beam walking test, following standard procedures (53,54). Hearing was evaluated by ABR analyses at two time points: five wt and six *Cldn14*$^{-/-}$ mice were tested at P15–P17; 10 mice of each genotype (*Cldn14*$^{-/-}$, *Cldn14*$^{+/-}$ and *Cldn14*$^{+/+}$) were tested at 4 weeks of age. Mice were anesthetized with intraperitoneal injection of 2.5% Avertin (0.015 ml/g body weight). All recordings were done in a sound-attenuated chamber using an auditory evoked potential diagnostic system (Intelligent Hearing Systems, Miami, FL) with high-frequency transducers, as previously described (82). Responses to 50 µs duration clicks, and 8, 16 and 32 kHz tone bursts were recorded. Thresholds were determined in 5 dB steps of decreasing stimulus intensity, until waveforms lost reproducible morphology. The maximum sound intensity tested for each frequency was 100 dB-SPL. EP measurements were performed on 5 and 10-week-old mice of all three genotypes as described (83).

Electron microscopy

Cochleae of *Cldn14*$^{-/-}$, *Cldn14*$^{+/-}$ and *Cldn14*$^{+/+}$ mice ranging from P7 to P18 were obtained and processed for SEM as described (84). Freeze fracture replicas were obtained from basal and apical coils of P7 mice cochleae and processed for electron microscopy as described (85).

Immunohistochemistry and X-gal staining

Cochleae of *Cldn14*$^{-/-}$, *Cldn14*$^{+/-}$ and *Cldn14*$^{+/+}$ mice ranging from P7 to P18 were obtained and processed for immunohistochemistry with an antibody against the N-terminus of prestin (55). Immunolocalization of claudin 14 was performed on a cochlea of an 8-week-old C57Bl/6 mouse, as well as cochleae of P7 wt and *Cldn14*-null mice, with an antibody against claudin 14 (39). Rhodamine-phalloidin staining (Molecular Probes, Eugene, OR) was performed as described (84). Activity of the *lacZ* reporter gene product, β-galactosidase, was detected by whole mount X-gal staining (86). For all heterozygous samples stained with X-gal, corresponding samples from wt mice were processed simultaneously as controls for endogenous β-galactosidase activity. No staining was observed in these control samples.

Mouse OC cultures

OC cultures were prepared from cochleae of *Cldn14*$^{-/-}$, *Cldn14*$^{+/-}$ and *Cldn14*$^{+/+}$ mice at P3–P5 according to the procedure described (87) with some modifications. The cochleae were dissected in Leibowitz cell culture medium, L-15 (Invitrogen, Carlsbad, CA). The OC spiral was dissected away from the modiolus, stria and spiral ligament. The tectorial membrane was removed and the middle and apical turns of the OC were separated from the basal turns and cut into two pieces. Each piece was transferred and adhered to a glass bottom petri dish (MatTek Corp, Ashland, MD) coated with CellTak (Collaborative BioMedical Products, Bedford, MA) and filled with 2 ml of DMEM culture medium supplemented with 7% fetal bovine serum (Invitrogen, Carlsbad, CA). Cultures were maintained at 37°C and 5% CO_2 for several days up to either P10 or P14, and then fixed in 4% paraformaldehyde for 2 h at room temperature and processed for immunocytochemistry using the anti-prestin antibody and rhodamine-phalloidin as described previously.

MDCK cell cultures and electrophysiologic measurements

Full-length *CLDN14* cDNA was isolated from a human kidney cDNA library using standard PCR techniques and cloned into the pTRE vector (Clontech Laboratories Inc.). Multiple clonal lines were selected in the doxycycline repressible tet-off MDCK cell line (Clontech Laboratories Inc.), which were tightly

inducible and expressed claudin 14 in all cells. Antisera against human claudin 14 was raised in rabbits using the peptide QDEAPYRPYQAPPRA. Culture methods, immunoblotting, immunofluorescence microscopy and electrophysiologic measurements were performed as previously described (27,56).

ACKNOWLEDGEMENTS

We thank Richard Mulligan for the pPNT vector; Richard Palmiter for the pnlacf plasmid; Andras Nagi, Reka Nagi and Wanda Abramow-Newerly for the R1 ES cells; Bechara Kachar for the anti-prestin antibody; Jacqueline Crawley for the use of her rotarod instrument; Jessica Wolfman, Kim Laws and Gary Dootz for technical help; and Matthew Kelley, Doris Wu, Dennis Drayna, Andrew Griffith, Gregory Frolenkov and Robert Morell for critical reading of this manuscript. The Transgenic Animal Model Core is supported by P60AR20557, P30CA46592, the State of Michigan's Animal Model Consortium and the University of Michigan. This work was also supported by the intramural funds of the National Institute on Deafness and Other Communication Disorders (NIDCD) (1 Z01 DC 00039-06) to T.B.F. and extramural support NIDDK-DK45134 to J.M.A.

REFERENCES

1. Madara, J.L. (1998) Regulation of the movement of solutes across tight junctions. *Annu. Rev. Physiol.*, **60**, 143–159.
2. Anderson, J.M. (2001) Molecular structure of tight junctions and their role in epithelial transport. *News Physiol. Sci.*, **16**, 126–130.
3. Tsukita, S., Furuse, M. and Itoh, M. (2001) Multifunctional strands in tight junctions. *Nat. Rev. Mol. Cell Biol.*, **2**, 285–293.
4. Pinto da Silva, P. and Kachar, B. (1982) On tight-junction structure. *Cell*, **28**, 441–450.
5. Staehelin, L.A. (1974) Structure and function of intercellular junctions. *Int. Rev. Cytol.*, **39**, 191–283.
6. Cereijido, M., Valdes, J., Shoshani, L. and Contreras, R.G. (1998) Role of tight junctions in establishing and maintaining cell polarity. *Annu. Rev. Physiol.*, **60**, 161–177.
7. Dragsten, P.R., Blumenthal, R. and Handler, J.S. (1981) Membrane asymmetry in epithelia: is the tight junction a barrier to diffusion in the plasma membrane? *Nature*, **294**, 718–722.
8. van Meer, G. and Simons, K. (1986) The function of tight junctions in maintaining differences in lipid composition between the apical and the basolateral cell surface domains of MDCK cells. *EMBO J.*, **5**, 1455–1464.
9. van Meer, G., Gumbiner, B. and Simons, K. (1986) The tight junction does not allow lipid molecules to diffuse from one epithelial cell to the next. *Nature*, **322**, 639–641.
10. Furuse, M., Hirase, T., Itoh, M., Nagafuchi, A., Yonemura, S. and Tsukita, S. (1993) Occludin: a novel integral membrane protein localizing at tight junctions. *J. Cell Biol.*, **123**, 1777–1788.
11. Tsukita, S. and Furuse, M. (2000) Pores in the wall: claudins constitute tight junction strands containing aqueous pores. *J. Cell Biol.*, **149**, 13–16.
12. Martin-Padura, I., Lostaglio, S., Schneemann, M., Williams, L., Romano, M., Fruscella, P., Panzeri, C., Stoppacciaro, A., Ruco, L., Villa, A. *et al.* (1998) Junctional adhesion molecule, a novel member of the immunoglobulin superfamily that distributes at intercellular junctions and modulates monocyte transmigration. *J. Cell Biol.*, **142**, 117–127.
13. Williams, L.A., Martin-Padura, I., Dejana, E., Hogg, N. and Simmons, D.L. (1999) Identification and characterisation of human Junctional Adhesion Molecule (JAM). *Mol. Immunol.*, **36**, 1175–1188.
14. Nasdala, I., Wolburg-Buchholz, K., Wolburg, H., Kuhn, A., Ebnet, K., Brachtendorf, G., Samulowitz, U., Kuster, B., Engelhardt, B., Vestweber, D. *et al.* (2002) A transmembrane tight junction protein selectively expressed on endothelial cells and platelets. *J. Biol. Chem.*, **277**, 16294–16303.
15. Turner, J.R. (2000) 'Putting the squeeze' on the tight junction: understanding cytoskeletal regulation. *Semin. Cell Dev. Biol.*, **11**, 301–308.
16. Gonzalez-Mariscal, L., Betanzos, A. and Avila-Flores, A. (2000) MAGUK proteins: structure and role in the tight junction. *Semin. Cell Dev. Biol.*, **11**, 315–324.
17. Mitic, L.L., Van Itallie, C.M. and Anderson, J.M. (2000) Molecular physiology and pathophysiology of tight junctions I. Tight junction structure and function: lessons from mutant animals and proteins. *Am. J. Physiol. Gastrointest. Liver. Physiol.*, **279**, G250–254.
18. Ebnet, K., Suzuki, A., Horikoshi, Y., Hirose, T., Meyer Zu Brickwedde, M.K., Ohno, S. and Vestweber, D. (2001) The cell polarity protein ASIP/PAR-3 directly associates with junctional adhesion molecule (JAM). *EMBO J.*, **20**, 3738–3748.
19. Hamazaki, Y., Itoh, M., Sasaki, H., Furuse, M. and Tsukita, S. (2002) Multi-PDZ domain protein 1 (MUPP1) is concentrated at tight junctions through its possible interaction with claudin-1 and junctional adhesion molecule. *J. Biol. Chem.*, **277**, 455–461.
20. Kawabe, H., Nakanishi, H., Asada, M., Fukuhara, A., Morimoto, K., Takeuchi, M. and Takai, Y. (2001) Pilt, a novel peripheral membrane protein at tight junctions in epithelial cells. *J. Biol. Chem.*, **276**, 48350–48355.
21. Nishimura, M., Kakizaki, M., Ono, Y., Morimoto, K., Takeuchi, M., Inoue, Y., Imai, T. and Takai, Y. (2002) JEAP, a novel component of tight junctions in exocrine cells. *J. Biol. Chem.*, **277**, 5583–5587.
22. Roh, M.H., Liu, C.J., Laurinec, S. and Margolis, B. (2002) The carboxyl terminus of zona occludens-3 binds and recruits a Mammalian homologue of discs lost to tight junctions. *J. Biol. Chem.*, **277**, 27501–27509.
23. Morita, K., Furuse, M., Fujimoto, K. and Tsukita, S. (1999) Claudin multigene family encoding four-transmembrane domain protein components of tight junction strands. *Proc. Natl Acad. Sci. USA*, **96**, 511–516.
24. Furuse, M., Sasaki, H. and Tsukita, S. (1999) Manner of interaction of heterogeneous claudin species within and between tight junction strands. *J. Cell Biol.*, **147**, 891–903.
25. Furuse, M., Furuse, K., Sasaki, H. and Tsukita, S. (2001) Conversion of zonulae occludentes from tight to leaky strand type by introducing claudin-2 into Madin-Darby canine kidney I cells. *J. Cell Biol.*, **153**, 263–272.
26. Tsukita, S. and Furuse, M. (2002) Claudin-based barrier in simple and stratified cellular sheets. *Curr. Opin. Cell Biol.*, **14**, 531.
27. Van Itallie, C., Rahner, C. and Anderson, J.M. (2001) Regulated expression of claudin-4 decreases paracellular conductance through a selective decrease in sodium permeability. *J. Clin. Invest.*, **107**, 1319–1327.
28. Sonoda, N., Furuse, M., Sasaki, H., Yonemura, S., Katahira, J., Horiguchi, Y. and Tsukita, S. (1999) Clostridium perfringens enterotoxin fragment removes specific claudins from tight junction strands: Evidence for direct involvement of claudins in tight junction barrier. *J. Cell Biol.*, **147**, 195–204.
29. Gregory, M., Dufresne, J., Hermo, L. and Cyr, D. (2001) Claudin-1 is not restricted to tight junctions in the rat epididymis. *Endocrinology*, **142**, 854–863.
30. Nishiyama, K., Sakaguchi, H., Hu, J.G., Bok, D. and Hollyfield, J.G. (2002) Claudin localization in cilia of the retinal pigment epithelium. *Anat. Rec.*, **267**, 196–203.
31. Brizuela, B.J., Wessely, O. and De Robertis, E.M. (2001) Overexpression of the Xenopus tight-junction protein claudin causes randomization of the left-right body axis. *Dev. Biol.*, **230**, 217–229.
32. Kollmar, R., Nakamura, S.K., Kappler, J.A. and Hudspeth, A.J. (2001) Expression and phylogeny of claudins in vertebrate primordia. *Proc. Natl Acad. Sci. USA*, **98**, 10196–10201.
33. Simon, D.B., Lu, Y., Choate, K.A., Velazquez, H., Al-Sabban, E., Praga, M., Casari, G., Bettinelli, A., Colussi, G., Rodriguez-Soriano, J. *et al.* (1999) Paracellin-1, a renal tight junction protein required for paracellular Mg2+ resorption. *Science*, **285**, 103–106.
34. Hirano, T., Kobayashi, N., Itoh, T., Takasuga, A., Nakamaru, T., Hirotsune, S. and Sugimoto, Y. (2000) Null mutation of PCLN-1/Claudin-16 results in bovine chronic interstitial nephritis. *Genome Res.*, **10**, 659–663.
35. Hirano, T., Hirotsune, S., Sasaki, S., Kikuchi, T. and Sugimoto, Y. (2002) A new deletion mutation in bovine Claudin-16 (CL-16) deficiency and diagnosis. *Animal Genet.*, **33**, 118–122.
36. Gow, A., Southwood, C.M., Li, J.S., Pariali, M., Riordan, G.P., Brodie, S.E., Danias, J., Bronstein, J.M., Kachar, B. and Lazzarini, R.A. (1999) CNS myelin and sertoli cell tight junction strands are absent in Osp/claudin-11 null mice. *Cell*, **99**, 649–659.
37. Furuse, M., Hata, M., Furuse, K., Yoshida, Y., Haratake, A., Sugitani, Y., Noda, T., Kubo, A. and Tsukita, S. (2002) Claudin-based tight junctions are crucial for the mammalian epidermal barrier: a lesson from claudin-1-deficient mice. *J. Cell Biol.*, **156**, 1099–1111.

38. Turksen, K. and Troy, T.C. (2002) Permeability barrier dysfunction in transgenic mice overexpressing claudin 6. *Development*, **129**, 1775–1784.
39. Wilcox, E.R., Burton, Q.L., Naz, S., Riazuddin, S., Smith, T.N., Ploplis, B., Belyantseva, I., Ben-Yosef, T., Liburd, N.A., Morell, R.J. *et al.* (2001) Mutations in the gene encoding tight junction claudin-14 cause autosomal recessive deafness DFNB29. *Cell*, **104**, 165–172.
40. Ferrary, E. and Sterkers, O. (1998) Mechanisms of endolymph secretion. *Kidney Int. Suppl.*, **65**, S98–103.
41. Ryan, A.F., Wickham, M.G. and Bone, R.C. (1979) Element content of intracochlear fluids, outer hair cells, and stria vascularis as determined by energy-dispersive roentgen ray analysis. *Otolaryngol. Head Neck Surg.*, **87**, 659–665.
42. Johnstone, B.M., Patuzzi, R., Syka, J. and Sykova, E. (1989) Stimulus-related potassium changes in the organ of Corti of guinea-pig. *J. Physiol.*, **408**, 77–92.
43. Konishi, T. and Salt, A.N. (1983) Electrochemical profile for potassium ions across the cochlear hair cell membranes of normal and noise-exposed guinea pigs. *Hear. Res.*, **11**, 219–233.
44. Wangemann, P., Liu, J. and Marcus, D.C. (1995) Ion transport mechanisms responsible for K^+ secretion and the transepithelial voltage across marginal cells of stria vascularis *in vitro*. *Hear. Res.*, **84**, 19–29.
45. Wangemann, P. (1995) Comparison of ion transport mechanisms between vestibular dark cells and strial marginal cells. *Hear. Res.*, **90**, 149–157.
46. Wangemann, P. (2002) K(+) cycling and the endocochlear potential. *Hear. Res.*, **165**, 1–9.
47. Marcus, D.C., Wu, T., Wangemann, P. and Kofuji, P. (2002) KCNJ10 (Kir4.1) potassium channel knockout abolishes endocochlear potential. *Am. J. Physiol. Cell Physiol.*, **282**, C403–407.
48. Salt, A.N., Melichar, I. and Thalmann, R. (1987) Mechanisms of endocochlear potential generation by stria vascularis. *Laryngoscope*, **97**, 984–991.
49. Hudspeth, A.J. (1989) How the ear's works work. *Nature*, **341**, 397–404.
50. Evans, B.N. and Dallos, P. (1993) Stereocilia displacement induced somatic motility of cochlear outer hair cells. *Proc. Natl Acad. Sci. USA*, **90**, 8347–8351.
51. Jahnke, K. (1975) The fine structure of freeze-fractured intercellular junctions in the guinea pig inner ear. *Acta Otolaryngol. Suppl.*, **336**, 1–40.
52. Nagy, A., Rossant, J., Nagy, R., Abramow-Newerly, W. and Roder, J.C. (1993) Derivation of completely cell culture-derived mice from early-passage embryonic stem cells. *Proc. Natl Acad. Sci. USA*, **90**, 8424–8428.
53. Carter, J., Morton, J.A. and Dunnet, S.B. (1997) Motor coordination and balance in rodents. In Crawley, J.N., Rogawski, M.A., Sibley, D.R., Skolnik, P. and Wray, S. (eds), *Current Protocols in Neuroscience.* John Wiley and Sons, Inc., New York, Vol. 2, pp. 8.12.11–18.12.14.
54. Crawley, J.C. (2000) *What's Wrong with my Mouse? Behavioral Phenotyping of Transgenic and Knockout Mice.* Wiley-Liss, New York.
55. Belyantseva, I.A., Adler, H.J., Curi, R., Frolenkov, G.I. and Kachar, B. (2000) Expression and localization of prestin and the sugar transporter GLUT-5 during development of electromotility in cochlear outer hair cells. *J. Neurosci.*, **20**, RC116.
56. Colegio, O.R., Van Itallie, C.M., McCrea, H.J., Rahner, C. and Anderson, J.M. (2002) Claudins create charge-selective channels in the paracellular pathway between epithelial cells. *Am. J. Physiol. Cell Physiol.*, **283**, C142–147.
57. Furuse, M., Fujita, K., Hiiragi, T., Fujimoto, K. and Tsukita, S. (1998) Claudin-1 and -2: novel integral membrane proteins localizing at tight junctions with no sequence similarity to occludin. *J. Cell Biol.*, **141**, 1539–1550.
58. Kiuchi-Saishin, Y., Gotoh, S., Furuse, M., Takasuga, A., Tano, Y. and Tsukita, S. (2002) Differential expression patterns of claudins, tight junction membrane proteins, in mouse nephron segments. *J. Am. Soc. Nephrol.*, **13**, 875–886.
59. Weber, S., Schlingmann, K.P., Peters, M., Nejsum, L.N., Nielsen, S., Engel, H., Grzeschik, K.H., Seyberth, H.W., Grone, H.J., Nusing, R. *et al.* (2001) Primary gene structure and expression studies of rodent paracellin-1. *J. Am. Soc. Nephrol.*, **12**, 2664–2672.
60. Florian, P., Amasheh, S., Lessidrensky, M., Todt, I., Bloedow, A., Ernst, A., Fromm, M. and Gitter, A.H. (2003) Claudins in the tight junctions of stria vascularis marginal cells. *Biochem. Biophys. Res. Commun.*, **304**, 5–10.
61. Dallos, P. and Harris, D. (1978) Properties of auditory nerve responses in absence of outer hair cells. *J. Neurophysiol.*, **41**, 365–383.
62. Ryan, A. and Dallos, P. (1975) Effect of absence of cochlear outer hair cells on behavioural auditory threshold. *Nature*, **253**, 44–46.
63. Legan, P.K., Lukashkina, V.A., Goodyear, R.J., Kossi, M., Russell, I.J. and Richardson, G.P. (2000) A targeted deletion in alpha-tectorin reveals that the tectorial membrane is required for the gain and timing of cochlear feedback. *Neuron*, **28**, 273–285.
64. Liberman, M.C., Gao, J., He, D.Z., Wu, X., Jia, S. and Zuo, J. (2002) Prestin is required for electromotility of the outer hair cell and for the cochlear amplifier. *Nature*, **419**, 300–304.
65. Zahraoui, A., Louvard, D. and Galli, T. (2000) Tight junction, a platform for trafficking and signaling protein complexes. *J. Cell Biol.*, **151**, F31–36.
66. Itoh, M., Furuse, M., Morita, K., Kubota, K., Saitou, M. and Tsukita, S. (1999) Direct binding of three tight junction-associated MAGUKs, ZO-1, ZO-2, and ZO-3, with the COOH termini of claudins. *J. Cell Biol.*, **147**, 1351–1363.
67. Balda, M.S. and Matter, K. (2000) The tight junction protein ZO-1 and an interacting transcription factor regulate ErbB-2 expression. *EMBO J.*, **19**, 2024–2033.
68. Traweger, A., Fuchs, R., Krizbai, I.A., Weiger, T.M., Bauer, H.C. and Bauer, H. (2002) The tight junction protein ZO-2 localizes to the nucleus and interacts with the hnRNP protein SAF-B. *J. Biol. Chem.*, **27**, 27.
69. Anniko, M. and Wroblewski, R. (1981) Elemental composition of the developing inner ear. *Ann. Otol. Rhinol. Laryngol.*, **90**, 25–32.
70. Schmidt, R.S. and Fernandez, C. (1963) Development of mammalian endocochlear potential. *J. Exp. Zool.*, **153**, 227–236.
71. Tasaki, I., Davis, H. and Eldredge, D.H. (1954) Exploration of cochlear potentials in guinea pig with a microelectrode. *J. Acoust. Soc. Am.*, **26**, 765–773.
72. Zenner, H.P. (1986) K^+-induced motility and depolarization of cochlear hair cells. Direct evidence for a new pathophysiological mechanism in Meniere's disease. *Arch. Otorhinolaryngol.*, **243**, 108–111.
73. Zenner, H.P., Reuter, G., Zimmermann, U., Gitter, A.H., Fermin, C. and LePage, E.L. (1994) Transitory endolymph leakage induced hearing loss and tinnitus: depolarization, biphasic shortening and loss of electromotility of outer hair cells. *Eur. Arch. Otorhinolaryngol.*, **251**, 143–153.
74. Boettger, T., Hubner, C.A., Maier, H., Rust, M.B., Beck, F.X. and Jentsch, T.J. (2002) Deafness and renal tubular acidosis in mice lacking the K-Cl co-transporter Kcc4. *Nature*, **416**, 874–878.
75. Voldrich, L. (1979) Noise-noise effect upon the spreading of the posttraumatic progressive necrosis in the organ of Corti. *Arch. Otorhinolaryngol.*, **222**, 169–173.
76. Forge, A. (1985) Outer hair cell loss and supporting cell expansion following chronic gentamicin treatment. *Hear. Res.*, **19**, 171–182.
77. Leonova, E.V. and Raphael, Y. (1997) Organization of cell junctions and cytoskeleton in the reticular lamina in normal and ototoxically damaged organ of Corti. *Hear. Res.*, **113**, 14–28.
78. Raphael, Y. and Altschuler, R.A. (1991) Reorganization of cytoskeletal and junctional proteins during cochlear hair cell degeneration. *Cell Motil. Cytoskeleton*, **18**, 215–227.
79. Tybulewicz, V.L., Crawford, C.E., Jackson, P.K., Bronson, R.T. and Mulligan, R.C. (1991) Neonatal lethality and lymphopenia in mice with a homozygous disruption of the c-abl proto-oncogene. *Cell*, **65**, 1153–1163.
80. Gross-Bellard, M., Oudet, P. and Chambon, P. (1972) Isolation of high-molecular-weight DNA from mammalian cells. *Eur. J. Biochem.*, **36**, 32.
81. Southern, E.M. (1975) Detection of specific sequences among DNA fragments separated by gel electrophoresis. *J. Mol. Biol.*, **98**, 503–517.
82. Zheng, Q.Y., Johnson, K.R. and Erway, L.C. (1999) Assessment of hearing in 80 inbred strains of mice by ABR threshold analyses. *Hear. Res.*, **130**, 94–107.
83. Raphael, Y., Kobayashi, K.N., Dootz, G.A., Beyer, L.A., Dolan, D.F. and Burmeister, M. (2001) Severe vestibular and auditory impairment in three alleles of Ames waltzer (av) mice. *Hear. Res.*, **151**, 237–249.
84. Beyer, L.A., Odeh, H., Probst, F.J., Lambert, E.H., Dolan, D.F., Camper, S.A., Kohrman, D.C. and Raphael, Y. (2000) Hair cells in the inner ear of the pirouette and shaker 2 mutant mice. *J. Neurocytol.*, **29**, 227–240.
85. Souter, M. and Forge, A. (1998) Intercellular junctional maturation in the stria vascularis: possible association with onset and rise of endocochlear potential. *Hear. Res.*, **119**, 81–95.
86. Wong, M.H., Rubinfeld, B. and Gordon, J.I. (1998) Effects of forced expression of an NH2-terminal truncated beta-Catenin on mouse intestinal epithelial homeostasis. *J. Cell Biol.*, **141**, 765–777.
87. Sobkowicz, H.M., Bereman, B. and Rose, J.E. (1975) Organotypic development of the organ of Corti in culture. *J. Neurocytol.*, **4**, 543–572.